PRACE INSTYTUTU ODLEWNICTWA
TRANSACTIONS OF FOUNDRY RESEARCH INSTITUTE

Volume LVII Year 2017 Number 4

High temperature corrosion of metallic materials in coal fired power plant boilers

Tomasz Dudziak[1]

[1]*Foundry Research Institute, ul. Zakopiańska 73, 30-418 Krakow, Poland*

E-mail: tomasz.dudziak@iod.krakow.pl

Received: 06.10.2017. Accepted in revised form: 29.12.2017.

DOI: 10.7356/iod.2017.26

Abstract

The aim of this work was to perform high temperature tests in steam conditions at 700−800°C for 3000 hours. In this work seven alloys were studied: Cr rich austenitic steels 309S, 310S, HR3C, and two solid-solution strengthened Ni based alloys; Haynes® 230®, 617 alloy and two (γ') gamma-prime strengthened Ni based alloys; 263 and Haynes® 282®. The obtained results suggest that the exposed materials show high corrosion resistance under steam oxidation conditions where predominantly Cr_2O_3 and $MnCr_2O_4$ compounds developed. The materials showed no chromia evaporation process and no exfoliation of the external oxide scale. However, two (γ') gamma-prime strengthened Ni based alloys showed a high degree of internal oxidation that increased with temperature.

Keywords: steam oxidation, high temperature, austenitic steel, Ni based alloy

1. Introduction

Since the industrial revolution world energy demands have grown rapidly [1,2]. Energy consumption is expected to rise by approximately 49% by the end of 2035 [3]. The economies of developing countries are strongly dependent on electrical energy [1,4], with the main sources being conventional power plants of which ~40% are coal-fired units [3]. There are a variety of coal-fired power plant designs which have different operating conditions and thus have different energy generation efficiencies [5,6,7,8]. Power plant efficiency is strongly correlated to steam temperature and pressure, which is explained thermodynamically by the Carnot cycle (Ideal cycle) [9]. Since the efficiency of the Carnot cycle is defined as $(T_{max} - T_{min})/T_{max}$, where T_{max} is the maximum temperature in the thermodynamic cycle and T_{min} is minimum temperature, the most practical way to increase efficiency is to increase the maximum steam temperature [9,10,11]. Currently most of the coal-fired power plants operate with steam at temperatures around 580°C with pressures up to 24.3 MPa, which allows for efficiencies of 38−40%. In newly designed units the efficiency of energy generation is above 40% due to higher steam conditions (600−620°C) [6]. The most efficient power plants, currently in development are expected to have efficiencies in the range of 44−46% using the following steam conditions: 700−760°C and 36.5−38.5 MPa [12,13]. In order to generate energy from steam more efficiently, there is a need to identify high temperature resistant alloys which are able to withstand such steam conditions [14,15,16].

Alloys for such applications must have good high temperature oxidation resistance [17,18] and good thermal conductivity [19] in addition to good creep resistance [14]. Moreover good weldability [21]; fabricability [20]; and the ability to be coated [16] are considered as important factors. The severity of the higher steam conditions (temperature and pressure) increases the oxidation kinetics (oxidation rate) which results in thicker scale formation, faster metal loss and larger scale spallation [20,21]. As a consequence of which, the heat transfer within the boiler would be disturbed and tubes would overheat locally [23]. All these factors have an impact on the boiler durability, power plant operations and the general performance [22,23,24]. To mitigate those problems extensive research into high temperature steam oxidation is needed, with special consideration of temperature, time, alloy type, material composition and steam conditions (flow rates) [18,23]. There has been some research conducted for the ferritic and austenitic steels in the temperature range of 550−650°C [3,22,25,26,27] and nickel-based alloys in the temperature range of 700−800°C [3,22]; however such tests do not consider the impact of specimen geometry and steam flow. Literature shows that the oxide scale development in steam environments is dependent on the alloy composition (mainly chromium

content), steam exposure conditions (temperature, pressure) and the alloys microstructure/surface preparation. In general, the scales formed on ferritic steels are reported as having double-layered structures with (Cr,Fe) spinel as the inner and magnetite as the outer layer [28]. However, some researchers have found that a haematite layer is able to form as a third (outermost) layer on top of the magnetite layer, but this is dependent on the alloy type and the exposure conditions [29]. Austenitic steels with medium up to 20 wt. % Cr have also been reported to develop two layers; an inner metal spinel, the composition of which is dependent on the alloy type, and an outer magnetite layer [3,30]. In this paper, candidates for structural materials in power plant boilers are shown in the case of steam oxidation performance. In the study, austenitic steels 309S, 310S and HR3C with more than 20 wt. % Cr have been investigated in steam conditions together with two solid-solution strengthened alloys; Haynes® 230®, 617 alloy and two (γ') gamma-prime strengthened alloys; 263 and Haynes® 282®. The high temperature tests were conducted at 700−800°C for 3000 hours. Standard analytical procedures using Scanning Electron Microscopy (SEM), coupled with Energy Dispersive X-ray Spectroscopy (EDS) and X-ray Powder Diffraction (XRD) have been used to determine microstructural observations, chemical composition and phase development respectively.

2. Experimental procedure

2.1. Materials

In total, seven alloys were exposed; two solid-solution strengthened alloys; Haynes® 230®, 617 alloy; two gamma-prime (γ') strengthened materials; 263 alloy and Haynes® 282® and high alloyed steels rich in Cr: 309S, 310S and HR3C. Table 1 shows the nominal compositions according to producer certificates of the high-alloyed steels and Ni based alloys respectively.

Prior to steam testing at 700−800°C, materials were cut out from the plates in small squares (20 mm²). As mentioned, the HR3C alloy has been delivered as a tube section, the material has been machined into tube segments, which had dimensions of a ~15 mm length, ×10 mm width chord, with a 4 mm wall thickness. The surface of the steels and Ni based alloys was ground using 600 grit SiC paper. Furthermore, the samples were cleaned in acetone at 40°C for 15 min using an ultrasonic bath. Prior to and during the exposure, the samples were accurately weighed using a digital balance with a resolution of ±0.01 mg for masses $m \leq 80$ g. The digital balance (Sartorius CPA225D) was calibrated frequently using its internal calibration function and periodically with test weights. The oxidised samples in the first instance were characterised to investigate phase formation using a D500 Kristalloflex from Siemens with monochromatic X-ray sources Cu ($\lambda K\alpha$ = 1.54 A) and an X-ray diffractometer (XRD) (EMPYREAN Panalytical) with a Cu X-ray source using an Ni filter. Further steps of post exposure preparation of the samples after high temperature testing included, mounting of the samples in the conductive resin from Struers. The prepared materials where investigated using: FEI Scios ultra-high-resolution Dual Beam Scanning Electron Microscopy (SEM) in Backscatter Electron (BSE) mode, microanalyses were performed using a Silicon Drift Detector (SDD) in Energy X-ray spectrometry (EDS) with a standard resolution of 127 eV and an accelerating voltage of 25 kV.

2.2. Steam oxidation

The high temperature rig for Ni and Fe based alloy corrosion assessment is shown in Figure 1.

The rig consisted of a heat resistant furnace, where a reactive chamber made of 8 mm thick 316L stainless steel was used, inside the reactive chamber an Al_2O_3 5 mm thick ceramic liner was inserted. The Al_2O_3 liner prevents a steam oxidation reaction with the 316L stainless steel vessel reaction chamber under high temperature exposures. Hence, the Al_2O_3 liner in this work was responsible for the constant partial pressure of oxygen during high temperature tests. Deionised water throughout the system of polyamide cables and 304L stainless steel tubes was delivered by a peristaltic pump with a flow rate of 2.833 ml/min. Throughout the high temperature tests, deionised water in the reservoir was constantly purged by nitrogen in order to eliminate oxy-

Table 1. Chemical composition of the materials (wt. %) used in steam oxidation work

	Ni	Fe	Cr	Co	Mo	Si	Mn	Cu	Nb	La	Ti	Al	C	W	B	P	S	N
309S	14	Bal.	23	–	–	0.75	2.0	–	–	–	–	–	0.20	–	–	0.045	0.03	–
310S	21	Bal.	25	–	–	1.50	2.0	–	–	–	–	–	0.08	–	–	0.045	0.03	–
HR3C	20	Bal.	25	–	–	0.75	1.2	–	0.45	–	–	–	0.06	–	–	0.040	0.03	0.2
263 alloy	Bal.	0.6	20	20.0	6.0	0.40	0.6	0.2	–	–	1.2	0.6	0.06	–	–	–	–	–
617 alloy	Bal.	1.0	22	12.5	9.0	–	–	–	–	–	0.3	1.2	0.07	–	–	–	–	–
Haynes® 230®	Bal.	3.0	22	5.0	2.0	0.40	0.5	–	–	0.02	–	0.3	0.10	14	0.015	–	–	–
Haynes® 282®	Bal.	1.5	20	10.0	8.5	0.15	0.3	–	–	–	2.1	1.5	0.06	–	0.050	–	–	–

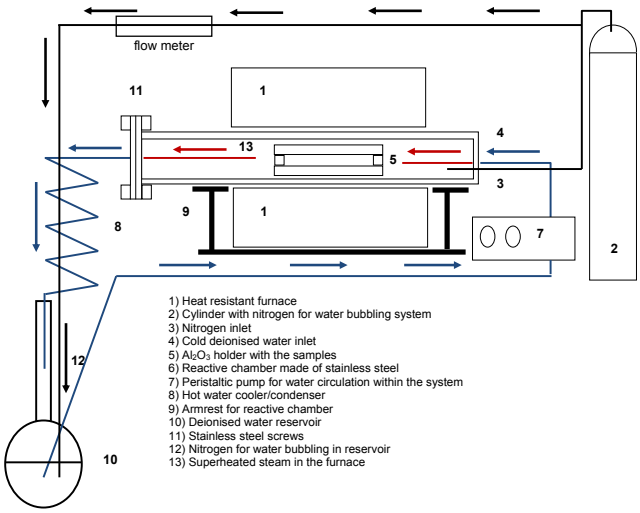

Fig. 1. Steam oxidation rig used in the experimental procedure

gen dissolved in the water from the ambient atmosphere (air). Nitrogen flow was constantly measured by a flow meter connected to the purging line. The samples were placed on the Al_2O_3 ceramic holder, and introduced into the furnace. The furnace was locked using 4 screws made of stainless steel. Additionally, when the chamber was closed, the nitrogen was run in order to purge the chamber and the samples for 2 hours at 200°C, to remove moisture and other impurities. Simultaneously, deionised water in the tank was constantly purged. Finally, when the temperature was nearing its maximum, nitrogen flow through the reactive chamber was turned off and a peristaltic pump was turned on to deliver deionised water to the reactive chamber. As mentioned, the tank with deionised water was constantly purged by nitrogen from a cylinder. When the test was finished, the peristaltic pump was turned off during the cooling period to prevent furnace inundation. Finally, the samples were removed at room temperature (20°C).

2.3. XRD investigations

Phase analyses were performed using two techniques; Bragg-Brentano (BB) geometry and the geometry of constant angle called grazing incidence using $\alpha = 1°$ and $\alpha = 3°$. In Bragg-Brentano (BB) geometry the penetration depth of the X-rays can be estimated using the following formula:

$$X = \frac{-\ln(1-Gx)\sin\theta}{2\mu} \quad (1)$$

where:

Gx – donates the intensity of the primary X-ray, giving important information related to irradiation volume,

μ – linear absorption coefficient.

In the grazing angle method, X-rays depth penetration can be calculated via the following formula:

$$X = \frac{-\ln(1-Gx)}{\left\{\mu\left[\frac{1}{\sin\alpha} + \frac{1}{\sin(2\theta-\alpha)}\right]\right\}} \quad (2)$$

where:

Gx – donates the intensity of the primary X-ray, giving important information related to irradiated volume, this value is equivalent to 0.95 (95%),

μ – linear absorption coefficient,

α – incidence angle.

The calculated values of Gx (assumption of Gx = 95%) are shown in Table 2.

Table 2. Depth penetration for the selected samples calculated using two different techniques

Sample/ phase	BB geometry, µm	Grazing incidence α = 1°, µm	Grazing incidence α = 3°, µm
309S	2.58–6.53	0.26	0.75
310S	2.89–7.32	0.29	0.84
HR3C	2.76–6.99	0.28	0.80
alloy 263	3.91–9.91	0.39	1.14
alloy 617	4.33–10.96	0.43	1.26
Haynes® 230®	4.23–10.71	0.42	1.23
Haynes® 282®	4.64–11.76	0.47	1.35

3. Results and discussion

3.1. Kinetic behaviour

Figure 2A–B and Figure 3A–B show mass gain data vs. time for the materials exposed at 700°C and 800°C for 3000 hours respectively.

The results clearly indicate that the materials exposed at 700°C showed much lower mass gain vs. time than the materials exposed at 800°C. In general, mass gain at 800°C was around 3 times higher than that observed at 700°C. Furthermore, both type of materials show similar high temperature corrosion behaviour: the exposed austenitic steels indicated static and constant mass gain, however the exposed Ni based alloys showed more scattered behaviour i.e. two gamma-prime (γ') strengthened materials; 263 alloy and Haynes® 282® at 700 and 800°C present-

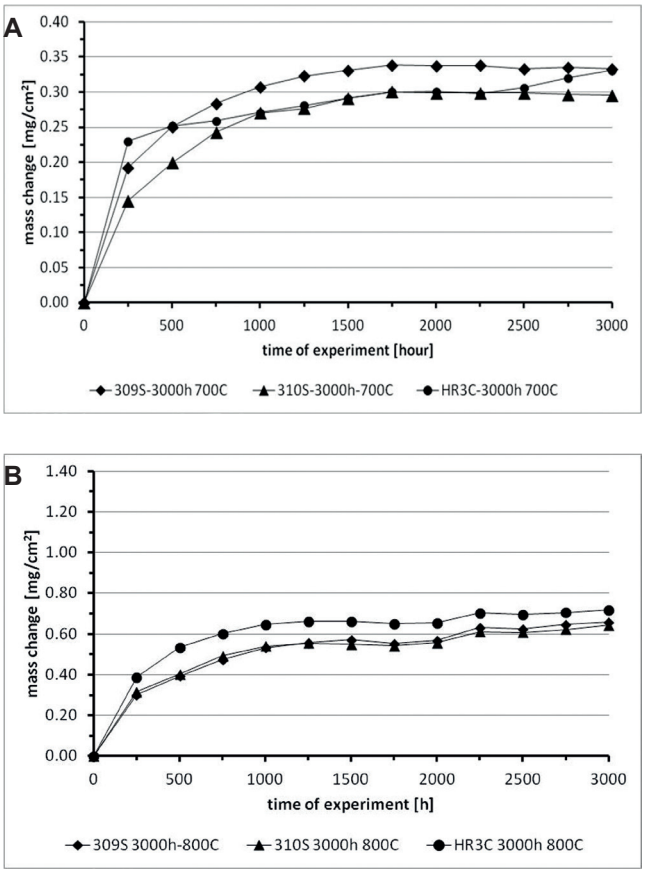

Fig. 2. Mass change vs. time for austenitic steels exposed at: A) 700°C and B) 800°C for 3000 hours in steam conditions

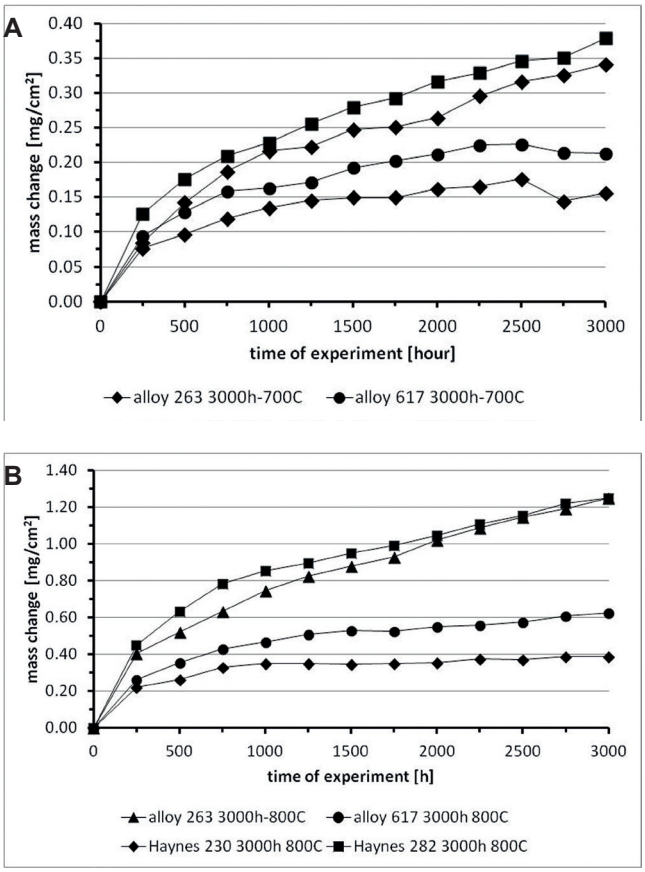

Fig. 3. Mass change vs. time for Ni based alloys at: A) 700°C and B) 800°C for 3000 hours in steam conditions

ed much higher mass gain. It is interesting to note, that the austenitic steel with the highest Cr content in metal matrix (HR3C) showed the highest mass gain from all of the exposed austenitic steels alike at 700°C and 800°C. Such behaviour can be explained based on the chemical composition of the 309S and the 310S steels where both steels contain higher Si content than the HR3C steel, it can therefore be assumed that a small addition of Si (up to 1.5 wt. %) may enhance corrosion behaviour of the Cr rich steel at high temperatures due to the formation of SiO_2 layer or, a similar compound containing Si within the oxide scale. In the past, some researchers postulated that the formation of SiO_2, or other Si containing compounds may enhance corrosion behaviour. Fry et al. [25] reported that for the mid Cr steels between 600−650°C exposures, Si additions positively influence kinetic behaviour, however has a negative effect, in that it encourages carbide agglomeration. Other researchers [31,32,33], have shown that increasing the content of Si from 0 to 1 wt. %, in 15 wt. % Cr steels increases time until breakaway oxidation due to the formation of a thin SiO_2 layer within the oxide scale. Based on the achieved results, it can be concluded that the current work also shows that Si addition to the metal matrix of highly alloyed steels positively influences high temperature corrosion behaviour in steam conditions.

The exposed Ni based alloys that have been heat treated under steam oxidation conditions beside Cr rich austenitic steels showed different behaviour. Two solid-solution strengthened Ni based alloys Haynes® 230®, 617 alloy in comparison to two (γ') gamma-prime strengthened Ni based alloys; 263 and Haynes® 282® showed much lower mass gain at both temperatures. The (γ') gamma-prime strengthened Ni based alloys indicated accelerated mass gain through the formation of fast growing phases. Particular attention is directed to the formation of TiO_2, which is a fast growing phase in oxygen rich atmospheres [34]. The formation of TiO_2 was reported earlier as well by Litz et al. [35], where researchers postulated the formation of an outer TiO_2 layer, an intermediate Cr_2O_3 layer with dissolved Ti, and an inner layer of (Ti, Nb, Ta)O_2 with a futile structure. Beneath the external scale an internal corrosion zone is formed that contains Al_2O_3 and TiN further into the substrate. In the current case, Ti originates from gamma-prime phase (γ'), hence higher mass gain has been observed for the alloys where gamma prime was present.

3.2. XRD analyses

Figure 4 and Figure 5 show XRD spectra obtained after investigations of the exposed and oxidised austenitic steels and Ni based alloys after the tests at 700 and 800°C for 3000 hours.

The XRD analyses carried out showed that the materials exposed to 700 and 800°C developed similar phases where mainly Cr_2O_3 and $MnCr_2O_4$ have been observed. Further, (γ') gamma-prime strengthened Ni based alloys; 263 and Haynes® 282® showed development of a fast growing TiO_2 phase. The solid solution strengthened Ni based alloy, 617, developed an oxide scale consisting of only two phases: Cr_2O_3 and $NiCr_2O_4$ instead of $MnCr_2O_4$.

The steels with Si additions (309S and 310S), formed Si rich phases such as: $(Mn,Fe)SiO_4$, SiO_2, and Mn_7SiO_{12} in addition to Fe_3O_4, however Fe_3O_4 was observed predominantly in the HR3C steel rather than in 309S or 310S. The results in this work are in agreement with other papers from the field of material science where Cr rich austenitic steels and Ni based alloys were tested. It has been suggested that those materials are prone to develop predominantly Cr_2O_3 and $MnCr_2O_4$ phases [36,37]. The investigation carried out, showed that in general, all of the exposed materials developed protective oxide scales under harsh conditions of steam oxidation, although Cr rich HR3C steel formed an Fe_3O_4 phase that is non-protective in comparison to Cr_2O_3 and is often observed in mid chromium steels such as T/P91 [38,39].

3.3. Microstructural observations

3.3.1. Surface

Figure 6 and Figure 7 present the microstructures of the exposed materials which were observed under SEM in BSE mode. The figures revealed that the exposed materials formed adherent oxide scales to the substrate with no detachment observed. Furthermore, it can be seen that the oxide scales developed at 800°C are coarser than those developed at 700°C, however, they still remain adherent to the metallic substrate.

3.3.2. Cross-section

Cross-sectional images of the exposed samples in BSE mode after exposures at 700 and 800°C are shown in Figure 8 and Figure 9 respectively. The figures present cross-sectional images captured after 3000 hours of oxidation in steam.

The presented results shown in Figure 8 and Figure 9 clearly demonstrate that the exposed materials underwent severe corrosion degradation especially at 800°C. As mentioned, corrosion resistance of the exposed materials was predominantly attributed to the formation of the Cr_2O_3 and $MnCr_2O_4$ external oxide scales. The highest performance among the exposed materials was observed in Haynes® 230® due to the lowest mass gain and the lowest internal oxidation rate. According to work published earlier, [40] for the same type of materials, it can be concluded that the solid-solution strengthened Ni based alloys; Haynes® 230®, 617 alloy indicate much better corrosion resistance than that offered by two gamma-prime (γ') strengthened alloys; 263 and Haynes® 282®. Two gamma-prime (γ') strengthened alloys; underwent a more severe corrosion degradation mainly due to oxidation of the gamma-prime (γ') phase and the formation of the extended internal oxidation region observed at 800°C. The process is primarily driven by the development of a fast growing TiO_2 phase. It is well known that the TiO_2 phase possesses a high number of defects in the crystal structure and is often responsible for accelerated mass gain in lightweight TiAl based alloys [41,42]. Kekare et al. [43] indicated that the doubly ionised oxygen vacancies are responsible for the kinetic rate of growth TiO_2 scales over Ti rich alloys and accelerated corrosion degradation. In this work the development of TiO_2 and Cr_2O_3 leads to accelerated ion flux according to the reaction below:

$Ti_{1+y}O_{2-y}$

Ti^{****}_i and $V^{\bullet\bullet}_o$ Ti (4 atoms in interstitials sites, double ionised vacancies)

$$Cr_2O_3 \longrightarrow Ti_{1+y}O_{2-y}$$

$$2Cr_2O_3 + Ti_{Ti} \longrightarrow 4Cr^{\bullet}_{Ti} + Ti^{****}_i + 6O_o$$

$$\longrightarrow Ti^{****}_i \uparrow$$

$$Cr_2O_3 + O_O \longrightarrow 2Cr'_{Ti} + V^{\bullet\bullet}_O + 4O_o$$

$$\longrightarrow V^{\bullet\bullet}_O \uparrow$$

Therefore, when developed TiO_2 as in this case is doped by Cr atoms, the process leads to the formation of a higher number of defects and enlargement of mass transport throughout point defects, hence this is a reason why two gamma-prime (γ') strengthened alloys; 263 and Haynes® 282® show much higher mass gain than the other two Ni based alloys and austenitic steels. Furthermore, it needs to be pointed out that alongside Cr_2O_3, a Mn_2O_4 spinel phase developed. The phase possesses a higher diffusion rate than that observed in Cr_2O_3, hence, this phenomena contributes extensively to higher corrosion rates in comparison to alloy 617 where no $MnCr_2O_4$ phase was identified, though the alloy showed the second best corrosion resistance. The proposed mechanism is a positive correlation with Cruchley et al. [16]. The researcher

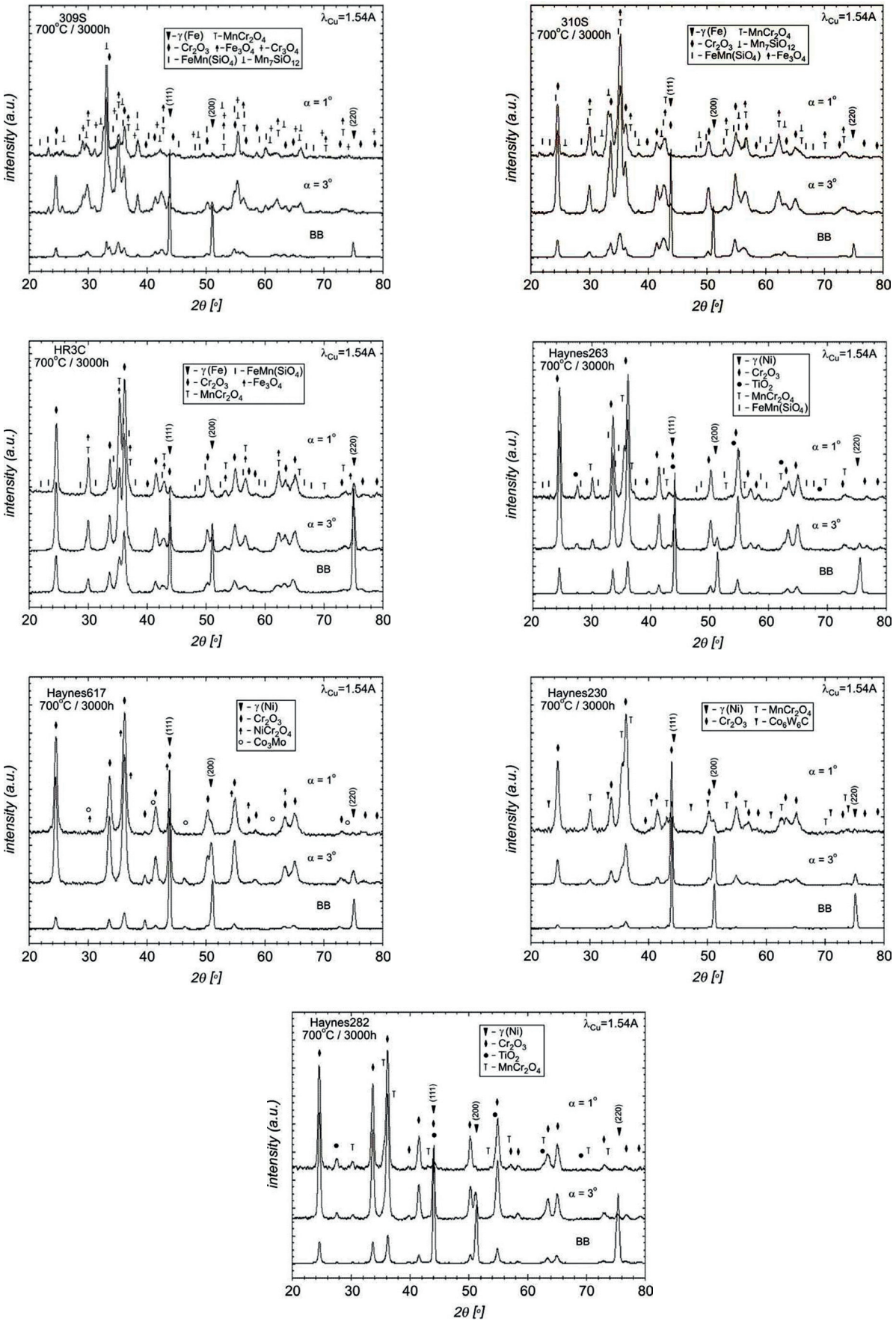

Fig. 4. XRD spectra of the exposed materials at 700°C for 3000 hours

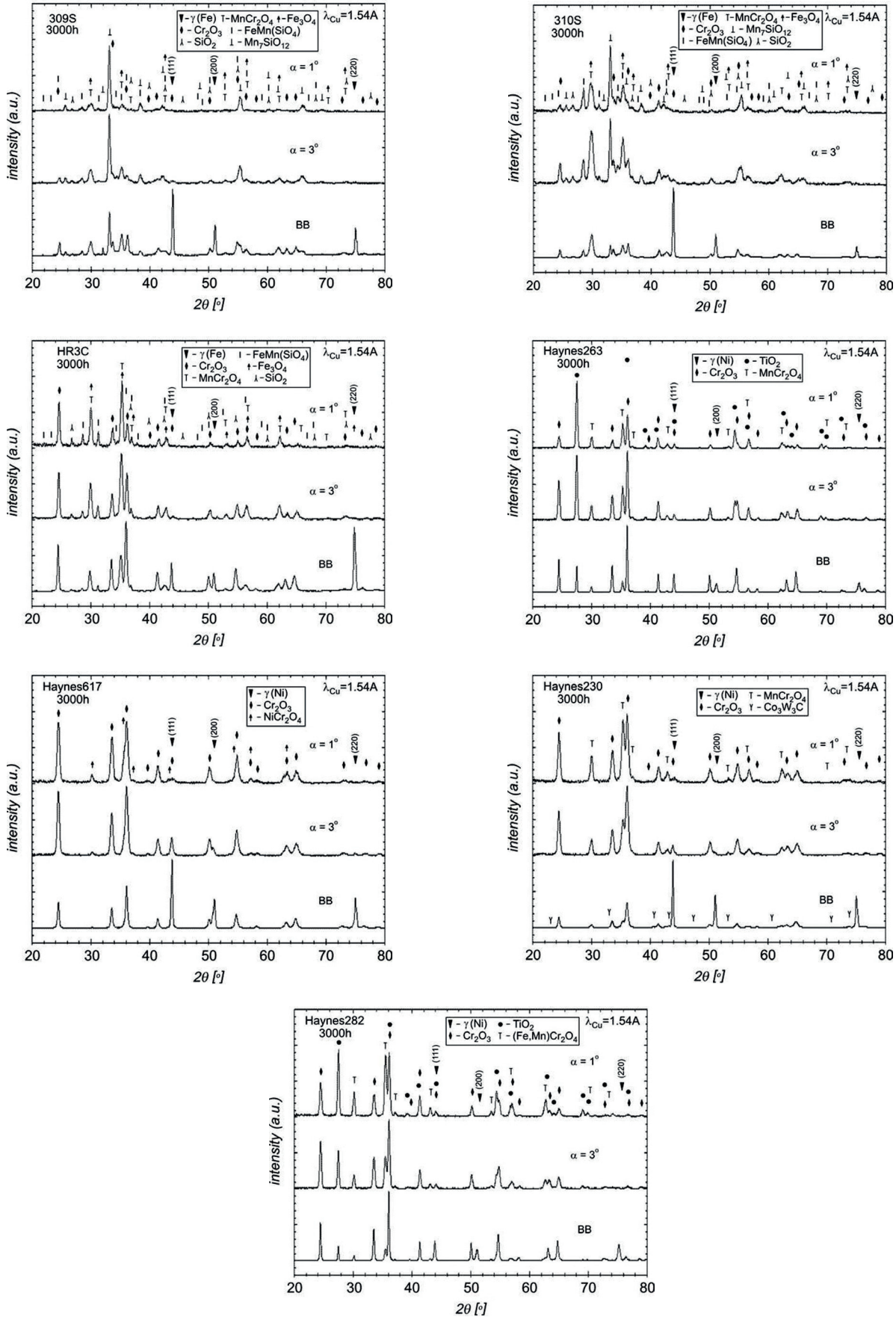

Fig. 5. XRD spectra of the exposed materials at 800°C for 3000 hours

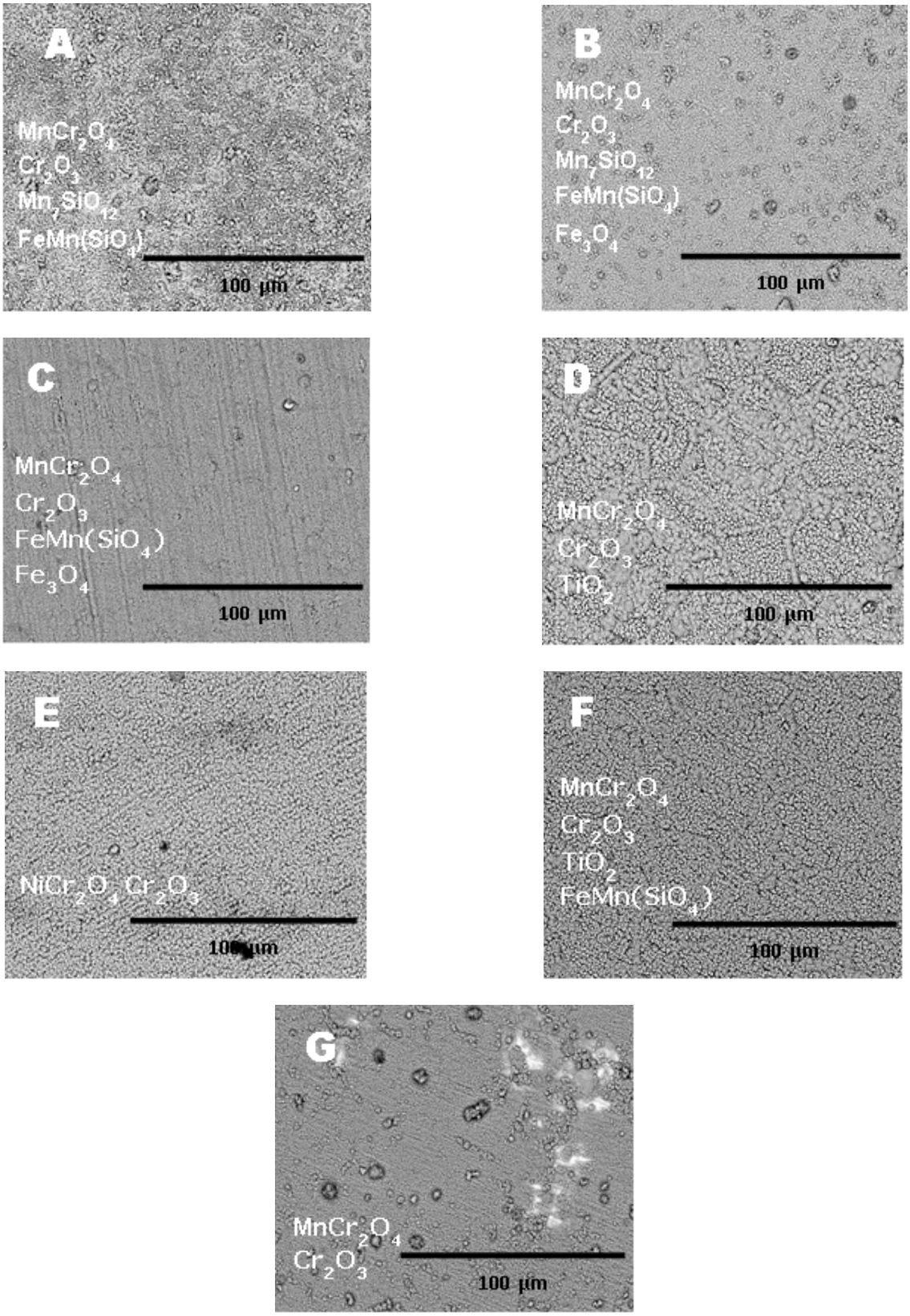

Fig. 6. Microstructures developed on the exposed materials in steam oxidation conditions at 700°C: A) 309S, B) 310S, C) HR3C, D) Haynes® 282®, E) alloy 617, F) 263 alloy, G) Haynes® 230®

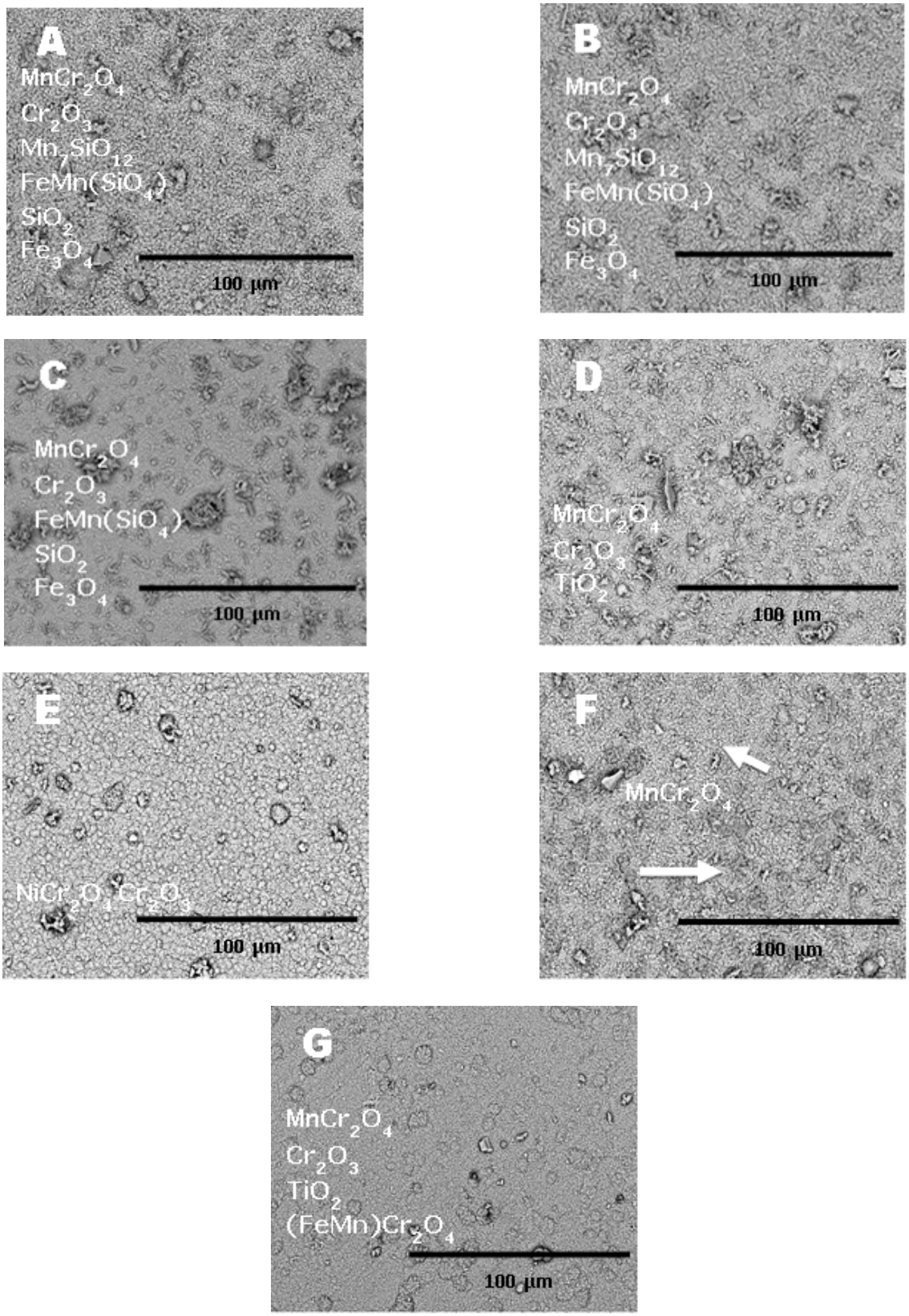

Fig. 7. Microstructures developed on the exposed materials in steam oxidation conditions at 800°C: A) 309S, B) 310S, C) HR3C, D) Haynes® 282®, E) alloy 617, F) 263 alloy, G) Haynes® 230®

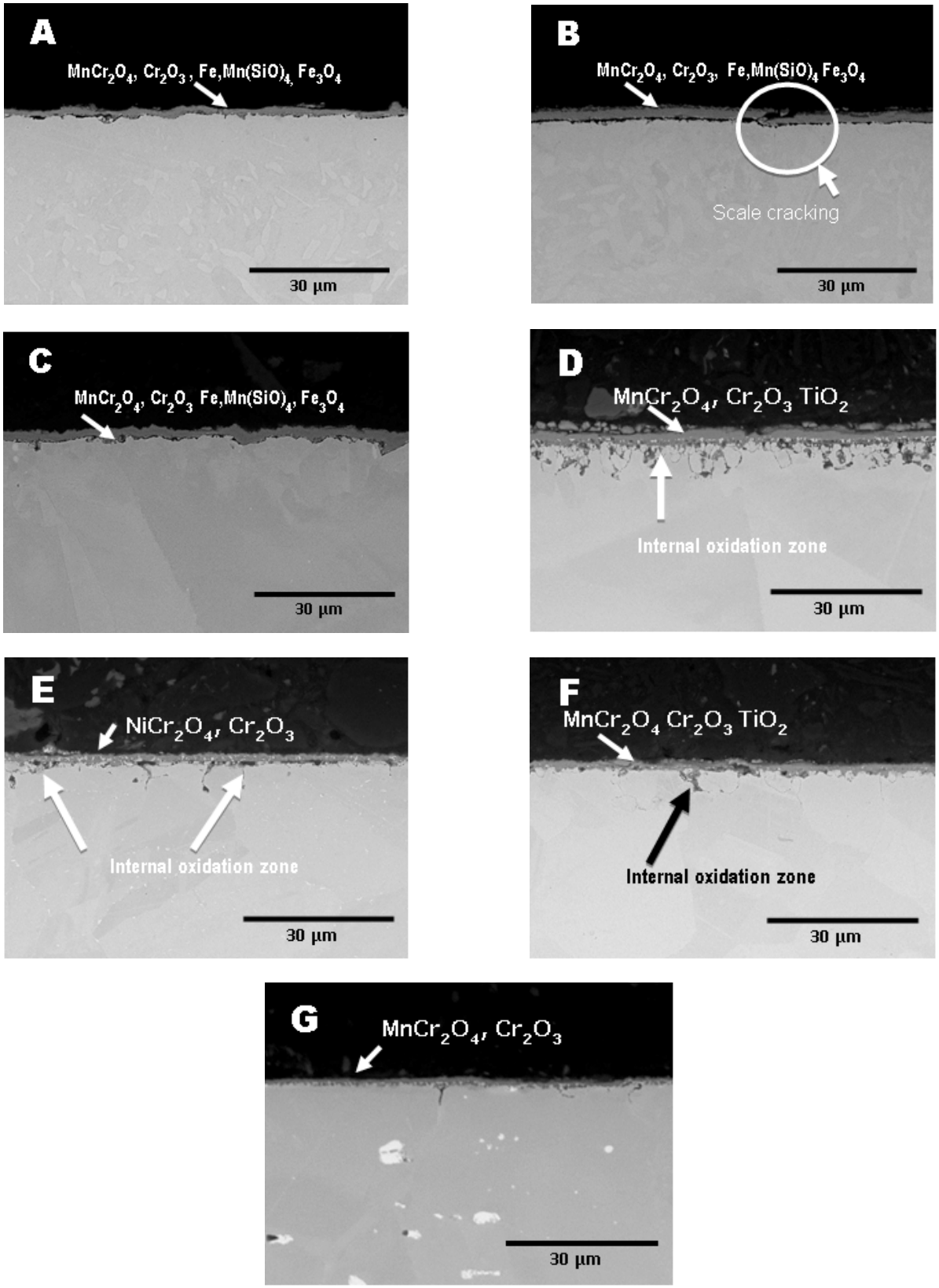

Fig. 8. Cross-sectioned microstructures developed on the exposed materials in steam oxidation conditions at 700°C: A) 309S, B) 310S, C) HR3C, D) Haynes® 282®, E) alloy 617, F) 263 alloy, G) Haynes® 230®

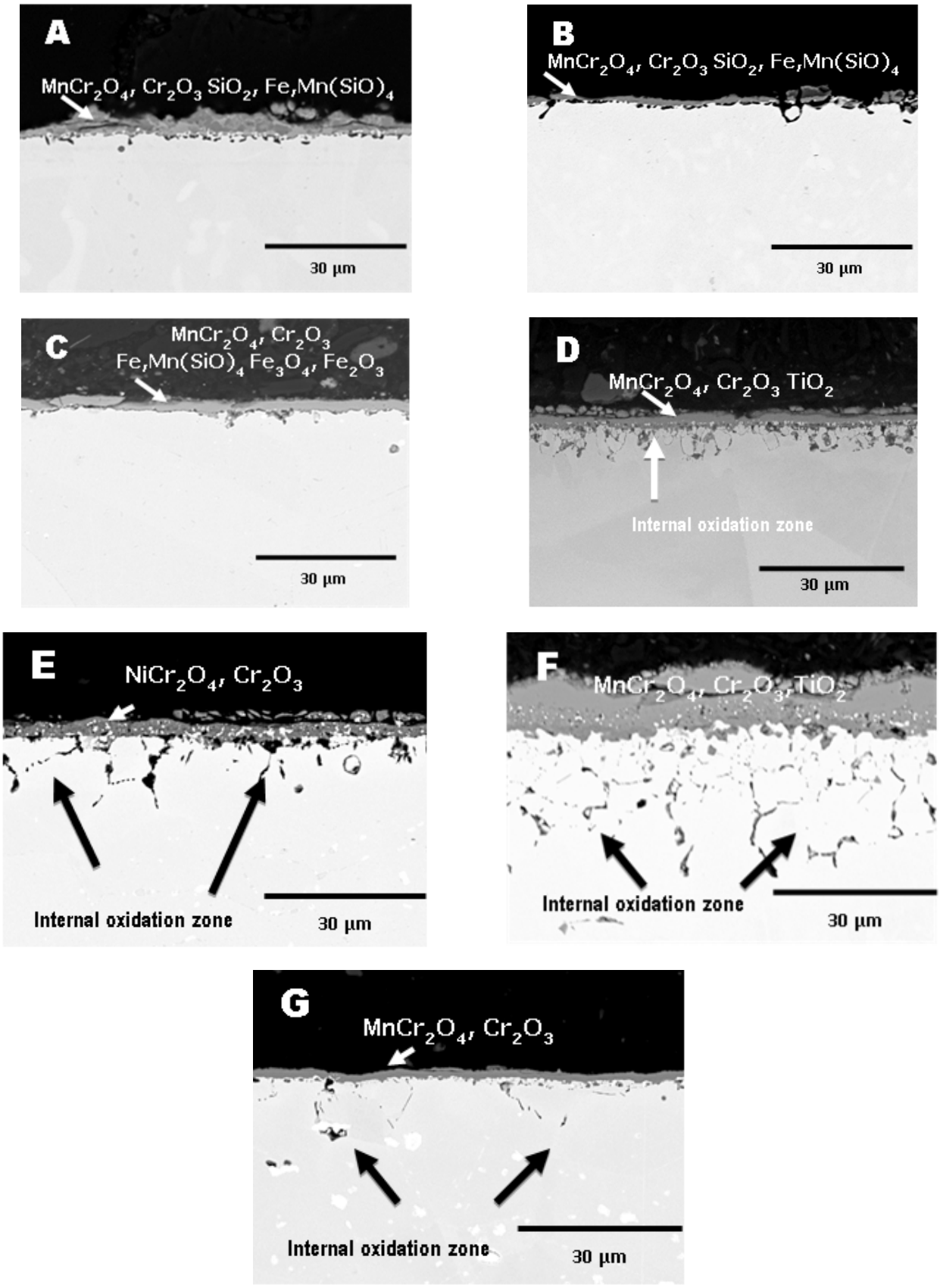

Fig. 9. Cross-sectioned microstructures developed on the exposed materials in steam oxidation conditions at 800°C: A) 309S, B) 310S, C) HR3C, D) Haynes® 282®, E) alloy 617, F) 263 alloy, G) Haynes® 230®

postulated that increased ionic transport is caused by doping of the chromia layer by titanium and the creation of vacancies on the chromium sub-lattice. Similarly to this research, researchers investigated the effect of Ti in Ni based alloys with an addition of Ti. It has been shown by Chen et al. [44], Kim et al. [45] and recently by Taylor et al. [46]. Furthermore, it has been found that Ti has a negative effect on the chromia scale due to the formation of a higher number of chromium vacancies which are responsible for higher diffusion rates of the chromium ion throughout the oxide scale. However, the concentration of Ti in the chromia scale is likely to reduce due to oxide scale thickening and depletion of Ti in the alloy. Finally, the internal oxidation process is in line with Al/Ti ratio in an alloy. Figure 10 shows column graphs where internal oxidation (μm) vs. Al + Ti is shown for the exposed materials at 700 and 800°C respectively.

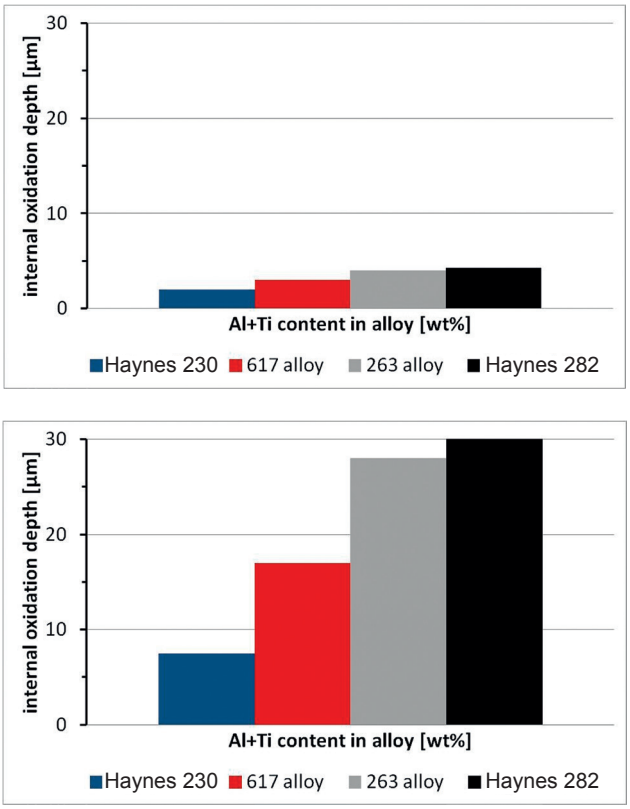

Fig. 10. Internal oxidation vs. Al + Ti concentration of the Ni based alloys exposed at: A) 700°C, B) 800°C) for 3000 hours in steam conditions

Figure 10 indicates that there is a direct relationship between Al and Ti content in a Ni based alloy and internal oxidation rate. The alloy with the lowest Al + Ti content shows the lowest internal oxidation rate (Haynes® 230®). In contrast, the alloy with the highest Al+Ti concentration indicates the highest internal oxidation rate (Haynes® 282®). The process is driven by the ability of Ti and Al to oxidise due to the high negativity of Gibbs free energy formation. In comparison to the other elements (Si, Ni, Cr, Mn) the formation of TiO_2 and Al_2O_3 requires as low as ΔG^O_T = −749.6 KJ·mol^{-1} and ΔG^O_T = −892.2 KJ·mol^{-1} energy to form an oxide, but the concentration of Al in the Haynes® 282® alloy compared to Ti concentration is much lower resulting in a much more prevalent formation of TiO_2 compared to Al_2O_3. Hence the alloy suffered from TiO_2 formation and development of point defects by the doping effect in Cr_2O_3 rich oxide scale.

The advanced steels rich in Cr and with small Si concentrations, when compared with Ni based alloys, showed slightly better corrosion resistance in terms of weight gain; furthermore, the steels showed no internal oxidation zone formation at 800°C. The observed corrosion resistance is attributed to the formation of Cr_2O_3, $MnCr_2O_3$. The role of those oxides in high temperature corrosion has been discussed many times earlier [25,47]. Henry et al. [32], and has shown that increasing the content of Si from 0 to 1 wt. %, in 15 wt. % Cr steel increases time until breakaway oxidation. Similarly, the addition of Si to 309S and 310S steels (> 20 wt. % Cr) may further enhance the breakaway process, not only because of high Cr content and high activity and Cr_2O_3, but also due to the effect of Si. The beneficial effects of Si in austenitic steel are clearly observed, the material with the highest Cr content showed higher mass gain, moreover, HR3C underwent a higher rate of nodule formation (not shown here) after long term exposure at high temperatures. The nodule formation indicates the formation of a less protective oxide scale and may lead to the initiation of breakaway oxidation [48]. In the case of 309S and 310S, some nodules have been observed as well but with a much lower rate, this phenomenon can be attributed to the formation of a thin inner SiO_2 rich layer or another Si containing phase that influence and reduce nodule formation on Cr rich austenitic steel.

4. Conclusions

The aim of this work was to perform a long term test at 700 and 800°C for 3000 hours and investigate corrosion behaviour of seven alloys: Cr rich austenitic steels 309S, 310S, HR3C, and two solid-solution strengthened Ni based alloys; Haynes® 230®, 617 alloy and two (γ') gamma-prime strengthened Ni based alloys; 263 and Haynes® 282®. The results lead to the conclusion that Cr rich austenitic steels and Ni based alloys developed thin adherent oxide scales at the lower temperature, whereas at the higher temperature more severe corrosion degradation was observed. The Ni based alloys with a gamma-prime (γ') phase show that this phase is responsible for extended internal oxidation rate, moreover the addition of Ti to the metal matrix and the high diffusion rate of Ti invoked a higher point defects rate and a higher corrosion process than that observed in

solid solution Ni based alloys. The austenitic steels with more than 20 wt. % Cr have shown adequate corrosion resistance, and a strong Si effect, however some nodules are formed especially in the steel with the highest Cr content but with the lowest Si concentration.

Acknowledgments

The authors would like to acknowledge the National Science Centre in Poland for the financial support of the fundamental research under the project number 2014/13/D/ST8/03256. Furthermore, the authors would like to acknowledge the following materials providers: Haynes International, Sandmeyer Steel Company and finally Institute for Ferrous Metallurgy in Poland for Ni based and advanced steels supply.

References

1. Rossa S. 2008. *Sustainable development handbook*. Lilbum: The Fairmont Press.

2. Boyle G., B. Everett, J. Ramage (eds.). 2003. *Energy systems and sustainability*. Oxford : Oxford University Press.

3. US Energy Information Administration. 2010. *International energy outlook 2010*. Washington DC: U.S. Department of Energy.

4. Sangster A.J. 2010. *Energy for a warming world. A plan to hasten the demise of fossil fuels*. Springer: London.

5. Kitto J. 1996. *Developments in pulverized coal-fired boiler technology*. Missouri Valley Electric Association Engineering Conference, 10−12 April 1996, Kansas City, Missouri, USA.

6. Nag P. 2008. *Power Plant Engineering*. New Delhi: Tata McGraw-Hill Publishing Company Limited.

7. Miller B.G. 2005. *Coal energy systems*. San Diego: Elsevier Academic Press.

8. Lindsley D. 2005. *Power-plant control and instrumentation: The control of boilers and HRSG systems*. London: The Institution of Electrical Engineers.

9. Müller I., W. Müller. 2009. *Fundamentals of thermodynamics and applications: With historical annotations and many citations from Avogadro to Zermelo*. Berlin Heidelberg: Springer-Verlag.

10. Wright I., P. Maziasz, F. Ellis, T. Gibbons, D. Woodford. 2004. *Materials Issues for turbines for operation in ultra-supercritical steam*. Clearwater: Proceedings of the 29th International Conference on Coal Utilization and Fuel Systems.

11. Massoud M. 2005. *Engineering thermofluids: Thermodynamic, fluid mechanics and heat tranfer*. Berlin Heidelberg: Springer-Verlag.

12. Gandy D., J. Shingledecker (eds.). 2013. *Advances in Materials Technology for Fossil Power Plants: Proceedings from the Seventh International Conference (EPRI 2013)*. Materials Park, Ohio: ASM International.

13. Bugge J., S. Kjær, R. Blum. 2006. “High-efficiency coal-fired power plants development and perspectives”. *Energy* 31 (10−11) : 1437−1445.

14. Viswanathan R., J. Sarver, J.M. Tanzosh. 2006. “Boiler materials for ultra-supercritical coal power plants – Steamside oxidation”. *Journal of Materials Engineering and Performance* 15 (3) : 255−274.

15. Viswanathan R., R. Purgert, U. Rao. 2002. *Materials technology for advance coal power plants*. Ohio: EPRI Meeting.

16. Cruchley S., H.E. Evans, M.P. Taylor, M.C. Hardy, S. Stekovic. 2013. “Chromia layer growth on a Ni-based superalloy: Sub-parabolic kinetics and the role of titanium”. *Corrosion Science* 75 : 58−66.

17. Ehlers J., D.J. Young, E. Smaardijk, A. Tyagi, H. Penkalla, L. Singheiser, W.J. Quadakkers. 2006. “Enhanced oxidation of the 9%Cr steel P91 in water vapour containing environments”. *Corrosion Science* 48 (11) : 3428−3454.

18. Maziasz P.J., I.G. Wright, J.P. Shingeldecker, R.R. Romanosky, T.B. Gibbons, F.V. Ellis, D.A. Woodford. 2005. Defining the materials issues and research for ultra-supercritical steam turbines, 602−622. In *Proceedings from the 4th International Conference, 25−28 October 2004*. Materials Park, Ohio: ASM International.

19. Laverde D., T. Gómez-Acebo, F. Castro. 2014. “Continuous and cyclic oxidation of T91 ferritic steel under steam”. *Corrosion Science* 46 (3) : 613−631.

20. Electric Power Research Institute. 2007. *Program on technology innovation: Oxide growth and exfoliation on alloys exposed to steam*. Palo Alto, California: EPRI Meeting.

21. Wright I.G., R.B. Dooley. 2010. “A review of the oxidation behaviour of structural alloys in steam”. *International Materials Reviews* 55 (3) : 129–167.

22. Lee N.-H., S. Kim, B.-H. Cheo, K.-B. Yoon, D. Kwon. 2009. “Failure analysis of a boiler tube in USC coal power plant”. *Engineering Failure Analysis* 16 (7) : 2031−2035.

23. Nishimura N., N. Komai, Y. Hirayama, F. Masuyama. 2005. “Japanese experience with steam oxidation of advanced heat-resistant steel tubes in power boilers”. *Materials at High Temperatures* 22 (1−2) : 3−10.

24. Komai N., F. Masuyama, M. Igarashi. 2005. “10-Year experience with T23(2.25Cr-1.6W) and T122(12Cr-0.4Mo-2W) in a power boiler”. *Journal of Pressure Vessel Technology* 127 (2) : 190−196.

25. Fry A., S. Osgerby, M. Wright. 2002. *Oxidation of Alloys in Steam Environments – A Review*. Teddington: National Physical Laboratory. NPL Report MATC(A)90.

26. Sarver J., J. Tanzosh. 2003. *Steam oxidation testing of candidate ultrasupercritical boiler materials*. Clearwater: 28th International Technical Conference on Coal Utilisation and Fuel Systems.

27. Saunders S., M. Monteiro, F. Rizzo. 2008. “The oxidation behaviour of metals and alloys at high temperatures in atmospheres containing water vapour: A review”. *Progress in Materials Science* 53 (5) : 775−837.

28. Hansson A., M. Montgomery. 2006. “Steam oxidation of TP 347H FG in power plants”. *Materials Science Forum* 522−523 : 181−188.

29. Hansson A.N., K. Pantleon, F.B. Grumsen, M.A.J. Somers. 2010. “Microstructure evolution during steam oxidation of a Nb stabilized austenitic stainless steel”. *Oxidation of Metals* 73 (1−2) : 289−309.

30. Dudziak T. EPSRC funded “SUPERGEN 2 – Conventional power plant lifetime extension”. Grant number EP/F029748/1.

31. Henry S., A. Galerie, L. Antoni. 2001. “Abnormal oxidation of stabilized ferritic stainless steels in water vapour”. *Materials Science Forum* 369−372 : 353−360.

32. Hurst P., H.C. Cowen. 1977. The oxidation of 9 Cr-Mo and other steels in 6.9 MN/m^2 steam at 748 and 823 K, paper 62. In *International Conference on Ferritic Steels for Fast Reactor Steam Generators*. London: British Nuclear Energy Society.

33. Griess J.C., W.A. Maxwell. 1981. “The long-term oxidation of selected alloys in superheated steam at 482 and 538°C”. Oak Ridge National Laboratory, ORNL-5771.

34. Reddy R.G., X. Wen, M. Divakar. 2001. “Isothermal oxidation of TiAl alloy”. *Metallurgical and Materials Transactions A* 32 (9) : 2357−2361.

35. Litz J., A. Rahmel, M. Schorr, J. Weiss. 1989. “Scale formation on the Ni-base superalloys IN 939 and IN 738 LC”. *Oxidation of Metals* 32 (3−4) : 167−184.

36. Gabrel J., C. Coussement, L. Verelst, R. Blum, Q. Chen, C. Testani. 2001. “Superheater materials testing for USC boilers: steam side oxidation rate of advanced materials in industrial conditions”. *Materials Science Forum* 369−372 : 931−938.

37. Deodeshmukh V.P. 2013. “Long-term performance of high-temperature foil alloys in water vapor containing environment. Part I: Oxidation behavior”. *Oxidation of Metals* 79 (5−6) : 567−578.

38. Yin K., S. Qiu, R. Tang, Q. Zhang, L. Zhang. 2009. “Corrosion behavior of ferritic/martensitic steel P92 in supercritical water”. *The Journal of Supercritical Fluids* 50 : 235−239.

39. Chen Y., K. Sridharan, T. Allen. 2006. “Corrosion behavior of ferritic-martensitic steel T91 in supercritical water”. *Corrosion Science* 48 (9) : 2843−2854.

40. Dudziak T., V. Deodeshmukh, L. Backert, N. Sobczak, M. Witkowska, W. Ratuszek, K. Chruściel, A. Zieliński, J. Sobczak, G. Bruzda. 2017. “Phase investigations under steam oxidation process at 800°C for 1000 h of advanced steels and Ni-based alloys”. *Oxidation of Metals* 87 (1−2) : 139−158.

41. Bjørheim T.S., A. Kuwabara, T. Norby. 2013. “Defect chemistry of rutile TiO_2 from first principles calculations”. *The Journal of Physical Chemistry C* 117 (11) : 5919−5930.

42. Du H.L., P.K. Datta, Z. Klusek, J.S. Burnell-Gray. 2004. “Nanoscale studies of the early stages of oxidation of a TiAl-base alloy”. *Oxidation of Metals* (62) 3−4 : 178−193.

43. Kekare S.A., P.B. Aswath. 1997. “Oxidation of TiAl based intermetallics”. *Journal of Materials Science* 32 (9) : 2485−2499.

44. Chen J.H., P.M. Rogers, J.A. Little. 1997. “Oxidation behavior of several chromia-forming commercial nickel-base superalloys”. *Oxidation of Metals* 47 (5−6) : 381−410.

45. Kim D., C. Jang, W.S. Ryu. 2009. “Oxidation characteristics and oxide layer evolution of alloy 617 and Haynes 230 at 900°C and 1100°C”. *Oxidation of Metals* 71 (5−6) : 271−293.

46. Taylor M.P., H.E. Evans, S. Stekovic, M.C. Hardy. 2012. “The oxidation characteristics of the nickel-based superalloy, RR1000, at temperatures of 700−900°C”. *Materials at High Temperatures* 29 : 145−150.

47. Othman N.K., N. Othman, J. Zhang, D.J. Young. 2009. “Effects of water vapour on isothermal oxidation of chromia-forming alloys in Ar/O_2 and Ar/H_2 atmospheres”. *Corrosion Science* 51 (12) : 3039–3049.

48. Evans H.E., A.T. Donaldson, T.C. Gilmour. 1999. “Mechanisms of breakaway oxidation and application to a chromia-forming steel”. *Oxidation of Metals* 52 (5−6) : 379−402.